Effects of Precursor Concentration and Acidic Sulfate in Aqueous Glyoxal−OH Radical Oxidation and Implications for Secondary Organic Aerosol

YI TAN,[†] MARK J. PERRI,[†] SYBIL P. SEITZINGER,[‡] AND BARBARA J. TURPIN*,[†]

Department of Environmental Sciences, Rutgers University, 14 College Farm Road, New Brunswick, New Jersey 08901, and Institute of Marine and Coastal Sciences, Rutgers University, 71 Dudley Road, New Brunswick, New Jersey 08901

Received June 14, 2009. Revised manuscript received September 8, 2009. Accepted September 29, 2009.

Previous experiments demonstrated that aqueous OH radical oxidation of glyoxal yields low-volatility compounds. When this chemistry takes place in clouds and fogs, followed by droplet evaporation (or if it occurs in aerosol water), the products are expected to remain partially in the particle phase, forming secondary organic aerosol (SOA). Acidic sulfate exists ubiquitously in atmospheric water and has been shown to enhance SOA formation through aerosol phase reactions. In this work, we investigate how starting concentrations of glyoxal (30−3000 μM) and the presence of acidic sulfate (0−840 μM) affect product formation in the aqueous reaction between glyoxal and OH radical. The oxalic acid yield decreased with increasing precursor concentrations, and the presence of sulfuric acid did not alter oxalic acid concentrations significantly. A dilute aqueous chemistry model successfully reproduced oxalic acid concentrations, when the experiment was performed at cloud-relevant concentrations (glyoxal <300 μM), but predictions deviated from measurements at increasing concentrations. Results elucidate similarities and differences in aqueous glyoxal chemistry in clouds and in wet aerosols. They validate for the first time the accuracy of model predictions at cloud-relevant concentrations. These results suggest that cloud processing of glyoxal could be an important source of SOA.

Introduction

Organic aerosols affect visibility, health, and global climate (*1, 2*). Current models underestimate organic aerosol concentrations in the free troposphere, suggesting there is a missing secondary organic aerosol (SOA) formation mechanism (*3, 4*). There is ample evidence suggesting that fog and cloud processing contributes to global SOA budget (*5*−*8*); however, our knowledge about the overall importance of fog and cloud processing to SOA formation is quite limited.

Fog and cloud processing, which is the dominant source of atmospheric sulfate, has been hypothesized to be a substantial source of SOA globally (*9, 10*). Briefly, reactive organic precursors are oxidized in the gas phase to form water-soluble products. These products readily partition into cloud droplets and react further with aqueous oxidants to form low-volatility compounds. Some reactions occur only in the aqueous phase (e.g., Russell mechanism of peroxyl radicals), and these reactions may lead to products not seen in gas phase chemistry. Upon cloud droplet evaporation, these low-volatility organics remain at least in part in the particle phase (e.g., 90% for oxalic acid), forming SOA (*11*). SOA could form through similar aqueous reactions in aerosol water as well.

Glyoxal is a common α-dicarbonyl formed in the atmospheric oxidation of biogenic and anthropogenic precursors, with a global source of 45 Tg a^{-1} (*12*). UV photolysis and reaction with the hydroxyl radical (OH) are primary gas phase loss processes for glyoxal (*13*). Glyoxal concentrations in the Mexico City atmosphere are found significantly below model predictions, suggesting existence of missing sinks (*14*). Reactive uptake of glyoxal by clouds and wet aerosols could plausibly explain this observation (*12*). Glyoxal can readily enter droplets because of a high effective Henry's law constant ($H_{eff} > 3 \times 10^5$ M atm^{-1} at 25 °C) and fast uptake rate (*15, 16*). Typical aqueous glyoxal concentrations vary from a few μM in rainwater to 276 μM in fogwater (*17*). Concentrations in wet aerosols could be several orders of magnitude higher. Aqueous oxidation of glyoxal forms low-volatility compounds, including oxalic acid and larger multifunctional products (*18*). In fact, aqueous formation from glyoxal and other carbonyl compounds helps explain the atmospheric abundance of oxalic acid and presence of oligomers in aerosols and clouds. Recent modeling suggests SOA through the aqueous reaction pathway is comparable in magnitude to other SOA formation pathways, though uncertainties are large (*12, 19*).

Sulfur(VI) contributes to the acidity of cloud droplets. Several studies suggest that sulfuric acid may participate in aerosol phase oligomerization reactions, including aldol condensation and hemiacetal−acetal formation (*20, 21*). However, the effect of acidic sulfate on SOA production through cloud processing has not been examined.

The kinetics of aqueous glyoxal OH radical oxidation have been studied by Carlton et al., but glyoxal concentrations in those experiments were 1−3 orders of magnitude higher than typical cloud and fog conditions (*18*). In this work, we investigate how the presence of acidic sulfate and starting concentrations of glyoxal affect product formation in bulk aqueous glyoxal OH radical experiments conducted at cloud-relevant pH. Some organic acids not previously identified in glyoxal oxidation were observed in these experiments as a result of improved analytical resolution. Reaction vessel kinetic modeling captured well product formation at cloud-relevant concentrations. Further chemical mechanism development is needed to improve SOA predictions from glyoxal in wet aerosols.

Experimental Section

Batch Reactions. Batch aqueous reactions of glyoxal and OH radical with and without sulfuric acid were conducted in a 1 L glass reaction vessel as described in detail elsewhere (*22*). The effect of two factors, glyoxal concentration and sulfuric acid concentration, on the production of low volatility compounds was studied. Experimental conditions are provided in Table S1 of the Supporting Information. Initial glyoxal concentrations were 30, 300, and 3000 μM, and H_2SO_4 concentrations were 0, 280, and 840 μM. The hydroxyl radical

* Corresponding author phone: 732-932-9800, extension 6219: fax: 732-932-8644; e-mail: turpin@envsci.rutgers.edu.
[†] Department of Environmental Sciences.
[‡] Institute of Marine and Coastal Sciences.

10.1021/es901742f CCC: $40.75
Published on Web 10/07/2009

(3×10^{-12} M to 6×10^{-12} M, estimated) was formed continuously by photolysis of H_2O_2, using a monochromatic (254 nm) mercury lamp (Heraeus Noblelight, Inc., Duluth, GA). Thus the OH radical concentration remained relatively constant, while the concentration of glyoxal decreased to 0 during experiments. All experiments were conducted at 25 ± 2 °C in duplicate. The pH varied from 5.2 to 2.1, decreasing with increasing H_2SO_4 and with increasing reaction time. Samples (10 mL) were taken at similar time points in each experiment with 10% duplicates. A 20 μL aliquot of a 1% catalase solution was added to each sample immediately to destroy H_2O_2. Batch reaction samples were analyzed within 12 h of collection by ion chromatography. Selected samples were also analyzed by mass spectral methods. One glyoxal experiment was performed with real-time mass spectral analysis as described in analytical methods.

The following control experiments were also conducted: glyoxal + UV, glyoxal + H_2SO_4, glyoxal + $H_2O_2 \pm H_2SO_4$, $H_2O_2 \pm H_2SO_4$ + UV, mixed standard + H_2O_2, and mixed standard + UV. The mixed standard contained oxalic, glyoxylic, malonic, succinic, formic, and glycolic acids. Pure water was also sampled from the reaction vessel and analyzed like samples.

The 30 μM glyoxal experiments are cloud relevant, and 300 μM experiments could represent some heavily polluted fogs. Glyoxal concentrations could reach extremely high values (~1−10 M) during cloud evaporation and in aerosol water. Examination of the chemistry with increasing glyoxal concentration provides some insights into differences between the aqueous photochemistry of glyoxal in cloud and aerosol water.

Online Experiments. ESI-MS online experiment (1000 μM glyoxal + 5 mM H_2O_2 + UV) was run as described by Perri et al. (*23*). The isocratic pump continuously delivered reaction solution from reaction vessel into ESI-MS at 0.11 mL/min, and the binary pump delivered mobile phase at 0.11 mL/min. Samples were analyzed in the negative ionization mode. Discrete samples were frozen for IC analysis.

Analytical Methods. Carboxylic acids were quantified by ion chromatography (IC) (ICS-3000, Dionex, Sunnyvale, CA) with an IonPac AS11-HC column (30 °C), AG11-HC guard column (Dionex, Synnyvale, CA), and conductivity detector (35 °C). A photodiode array detector provided additional product validation. Monovalent anions such as glycolate (5.9 min), formate (6.8 min), and glyoxylate (9.7 min) are only weakly retained. Bivalent ions such as succinate (20.4 min), malonate (21.5 min), and oxalate (24.6 min) elute after monovalent ions. Trivalent ions such as citrate are strongly retained and elute even later. Acetate and glycolate (5.9 min) and succinate and malate (20.4 min) as well as malonate and tartrate (21.5 min) coelute.

Fresh samples from batch experiments were analyzed by electrospray ionization mass spectrometry (ESI-MS) (HP-Agilent 1100) as described previously (*24*). ESI-MS is a soft ionization method that does not fragment ions. Carboxylic acids are detected in the negative ionization mode as molecular weight minus one ion because of the loss of an acidic proton. Aldehydes and alcohols are detected in the positive mode. Glyoxal is detected as m/z^+ 117 and 131 as previously reported. The ion m/z^+ 117 was used to qualitatively represent glyoxal in this work. A frozen sample (−20 °C) taken 30 min into the experiment (3000 μM glyoxal + OH radical; experiment 13, Table S1 of the Supporting Information) was analyzed by Fourier transform ion cyclotron resonance (FT-ICR) ESI-MS (Thermo-Finnigan LTQ-XL, Woods Hole Oceanographic Institute Mass Spectrometer Facility) to determine the elemental formulas of products from 95−500 amu (mass resolution 100 −750 k) as described by Perri et al. (*23*).

Selected samples were analyzed for total organic carbon, and hydrogen peroxide was measured in organic control experiments ($H_2O_2 \pm H_2SO_4$ + UV). Analytical details are provided in the Supporting Information.

Kinetic Modeling. Aqueous glyoxal photooxidation was modeled using a mechanism based on Lim et al. (*25*) (Table 1) and the differential solver, FACSIMILE (AEA Technology, Oxfordshire, U.K.). The H_2O_2 photolysis rate ($k = 1.1 \times 10^{-4}$ s^{-1}, reaction 1, Table 1) was fitted by simulating the H_2O_2 concentration in H_2O_2 + UV control experiments with reactions 1−5 (Table 1; Figure S1 of the Supporting Information). Modeled OH radical concentrations during the experiments were on average $3 \times 10^{-12} - 6 \times 10^{-12}$ M (Table S1 of the Supporting Information).

Quality Assurance/Quality Control (QA/QC). The expected products of glyoxal + OH radical are glyoxylic and oxalic acids. Neither glyoxal nor oxalic acid degraded in the presence of H_2O_2 alone (mixed standard + H_2O_2 control experiment). However, glyoxylic acid + H_2O_2 formed formic acid. To evaluate the effectiveness of catalase in destroying H_2O_2 in samples, we treated some samples from the mixed standard (pH 3.2) + H_2O_2 control experiment (10 mL) with 20 μL of a 1% catalase solution. Some H_2O_2 was still present in these samples after 5 min of contact with catalase. We believe the sample acidity inhibited catalase performance. The reaction of glyoxylic acid + H_2O_2 is slow compared to glyoxylic acid + OH radical (Table 1) *in the reaction vessel*. However, *in samples* OH radicals are instantly depleted. The destruction of H_2O_2 by catalase in these samples was not fast enough to prevent conversion of glyoxylic acid to formic acid prior to sample analysis in batch experiments. This explains the low glyoxylic acid concentrations measured by Carlton et al. (*18*) and suggests that formic and glyoxylic acid concentrations measured in batch experiments described here do not accurately reflect concentrations in the reaction vessel.

Data quality for organic acids is presented in detail in Table S2 and the text of the Supporting Information. Recoveries are near 100%, except for glyoxylic acid (86.5%). With the addition of H_2O_2, recoveries were unchanged for glycolic acid, malonic acid, succinic acid, and oxalic acid. However, glyoxylic acid disappeared, and formic acid concentration increased. Precision is better than 5% for all quantified organic acids.

Results and Discussion

Online Results. ESI-MS online analysis (Figure 1) demonstrates qualitative agreement with predictions (*25, 26*) and batch aqueous glyoxal + OH radical experiments conducted previously (*18*). Specifically, glyoxylic acid (m/z^- 73) is the first generation product. Oxalic acid (m/z^- 89) increased rapidly as glyoxylic acid decayed. The time profile of oxalic acid, quantified by IC, matches the abundance of m/z^- 89 (ESI-MS) very well. In agreement with previous batch experiments (*18*), a large number of additional ions were observed, including m/z^- 103, 117, 133, and 149, which will be discussed later. In previous batch experiments, the rapid appearance of formic acid (measured by IC) was taken to suggest that glyoxal + OH radical forms formic acid directly. As discussed in the previous section, we now know that glyoxylic acid reacts with residual H_2O_2 to form formic acid in collected samples from batch experiments. Because the ESI-MS cannot measure formic acid, this online experiment cannot be used to verify or refute the possibility that formic acid is formed directly from glyoxal.

Effect of Sulfuric Acid Addition. The addition of sulfuric acid had little effect on the oxalic acid production (Figure 2). Sulfuric acid appears to enhance oxalic acid decay slightly in the late stage of 30 μM experiments, and a slight suppression of oxalic acid production might occur at the

TABLE 1. Aqueous Reactions and Rate Constants in Glyoxal + OH Radical Model[a]

	reaction	rate constant (M^{-1} s^{-1})	footnote
1	$H_2O_2 + h\nu \rightarrow 2OH$	1.1×10^{-4}	*b*
2	$OH + H_2O_2 \rightarrow HO_2 + H_2O$	2.7×10^{7}	
3	$HO_2 + H_2O_2 \rightarrow OH + H_2O + O_2$	3.7	
4	$HO_2 + HO_2 \rightarrow H_2O_2 + O_2$	8.3×10^{5}	
5	$OH + HO_2 \rightarrow H_2O + O_2$	7.1×10^{9}	
6	$GLY + OH(+O_2) \rightarrow GLYAC + HO_2$	1.1×10^{9}	
7	$GLYAC + OH \rightarrow OXLAC + HO_2 + H_2O$	3.62×10^{8}	
8	$GLYAC^- + OH \rightarrow OXLAC^- + HO_2 + H_2O$	2.9×10^{9}	
9	$OXLAC + OH \rightarrow 2CO_2 + 2H_2O$	1.4×10^{6}	*c*
10	$OXLAC^- + OH \rightarrow CO_2 + CO_2^- + 2H_2O$	4.7×10^{7}	
11	$OXLAC^{2-} + OH \rightarrow CO_2 + CO_2^- + OH^-$	7.7×10^{6}	
12	$H_2O \leftrightarrow H^+ + OH^-$	$K_{eq} = 1.0 \times 10^{-14}$, $k_a = 1.4 \times 10^{11}$	
13	$HO_2 \leftrightarrow H^+ + O_2^-$	$K_{eq} = 1.6 \times 10^{-5}$, $k_a = 5.0 \times 10^{10}$	
14	$GLYAC \leftrightarrow H^+ + GLYAC^-$	$K_{eq} = 3.47 \times 10^{-4}$, $k_a = 2.0 \times 10^{10}$	
15	$OXLAC \leftrightarrow H^+ + OXLAC^-$	$K_{eq} = 5.67 \times 10^{-2}$, $k_a = 5.0 \times 10^{10}$	
16	$OXLAC^- \leftrightarrow H^+ + OXLAC^{2-}$	$K_{eq} = 5.42 \times 10^{-5}$, $k_a = 5.0 \times 10^{10}$	
17	$CO_2^- + O_2 \rightarrow O_2^- + CO_2$	2.4×10^{9}	
18	$GLYAC + H_2O_2 \rightarrow HCO_2H + CO_2 + H_2O$	0.3	*d*
19	$HCO_2H + OH \rightarrow CO_2 + HO_2 + H_2O$	1.0×10^{8}	
20	$HCO_2^- + OH \rightarrow CO_2^- + H_2O$	2.4×10^{9}	
21	$HCO_2H \leftrightarrow H^+ + HCO_2^-$	$K_{eq} = 1.77 \times 10^{-4}$, $k_a = 5.0 \times 10^{10}$	
22	$OH + O_2^- \rightarrow OH^- + O_2$	1×10^{10}	
23	$HCO_3^- + OH \rightarrow CO_3^- + H_2O$	1×10^{7}	
24	$CO_3^- + O_2^- \rightarrow CO_3^{2-} + O_2$	6.5×10^{8}	
25	$CO_3^- + HCO_2^- \rightarrow HCO_3^- + CO_2^-$	1.5×10^{5}	
26	$CO_3^- + H_2O_2 \rightarrow HCO_3^- + HO_2$	8×10^{5}	
27	$CO_2(+H_2O) \leftrightarrow H^+ + HCO_3^-$	$K_{eq} = 4.3 \times 10^{-7}$, $k_a = 5.6 \times 10^{4}$	
28	$HCO_3^- \leftrightarrow H^+ + CO_3^{2-}$	$K_{eq} = 4.69 \times 10^{-11}$, $k_a = 5 \times 10^{10}$	

[a] Reactions are taken from Lim et al. (*25*) and references therein except where footnoted. GLY = glyoxal, GLYAC = glyoxylic acid, OXLAC = oxalic acid, OH = OH radical. Dissociation rate constants (k_d, s^{-1}) are calculated from the equilibrium constant (K_{eq}, M) and association rate constants (k_a, M^{-1} s^{-1}) by $k_d = K_{eq} \times k_a$. [b] Hydrogen peroxide photolysis rate (k_1, s^{-1}) is estimated by fitting H_2O_2 loss in H_2O_2 + UV control experiments. [c] The reaction between oxalic acid and dissolved oxygen was removed from the initial mechanism as no reaction was observed in control experiments. [d] This reaction was measured by Leitzke et al. (*34*) and was not included by Lim et al.

beginning of 3000 μM experiments. Formation of organosulfur compounds is possible but is beyond the scope of this work.

Effect of Precursor Concentration. Increasing precursor concentrations resulted in a nonlinear decrease in the mass of oxalic acid (at maximum) per mass of glyoxal reacted, from 136% in 3000 μM experiments to 94% and 38% in 300 and 30 μM experiments, respectively (Figure 2, Table S1 of the Supporting Information). Also, the oxalic acid production was slower in 3000 μM experiments compared to lower concentration experiments. Most but not all of the decrease in the yield of oxalic acid with increasing precursor concentration is captured by the model results and reflects the fact that H_2O_2 concentrations are also much higher in the higher concentration experiments, whereas OH radical concentrations are only slightly larger. At the higher H_2O_2 concentrations, the formation of formic acid from glyoxylic acid and H_2O_2 competes with the formation of oxalic acid from glyoxylic acid and OH radical in the reaction vessel, reducing oxalic acid production. Oxalic acid did not form in

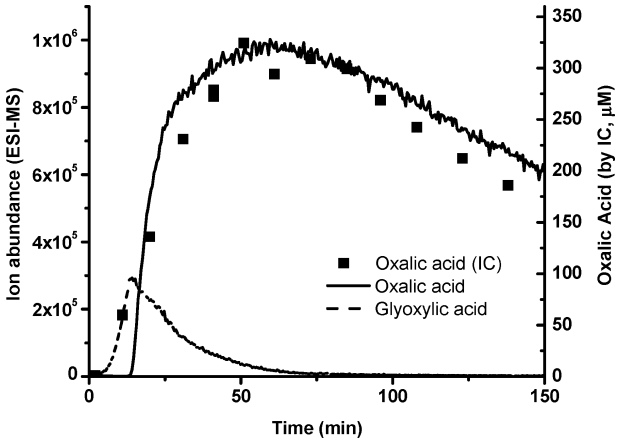

FIGURE 1. ESI-MS online analysis in negative scan mode of the glyoxal (1 mM) + OH radical (5 mM H_2O_2 + UV) experiment. Oxalic acid (m/z^- 89) and glyoxylic acid (m/z^- 73) are displayed in raw ion abundance from ESI-MS. Oxalic acid concentration quantified by IC is overlaid (■).

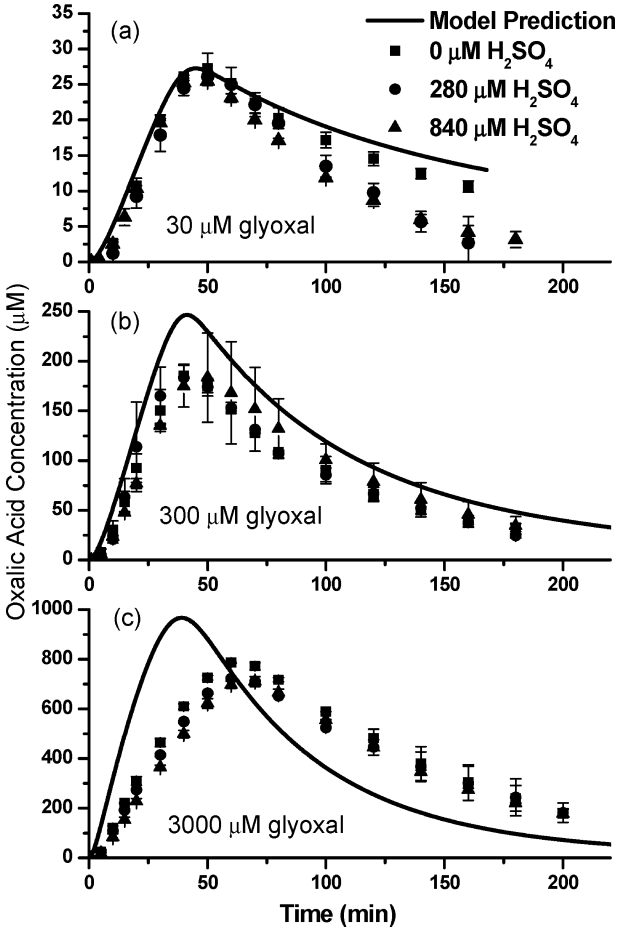

FIGURE 2. Oxalic acid time profiles from batch glyoxal ± H_2SO_4 + OH radical experiments and model predictions. Solid lines are modeled oxalic acid concentration, and data points are quantified concentrations from IC analysis. H_2SO_4 concentration in μM is given in legend. Experimental oxalic acid yields are listed in Table S1 of the Supporting Information.

control experiments (glyoxal + UV, glyoxal + H_2O_2). In glyoxal + OH radical experiments, glyoxal was completely consumed after 40 min as indicated by ESI-MS positive mode analysis (Supporting Information), and oxalic acid increased to a maximum concentration 40 − 70 min into the reaction. Peak

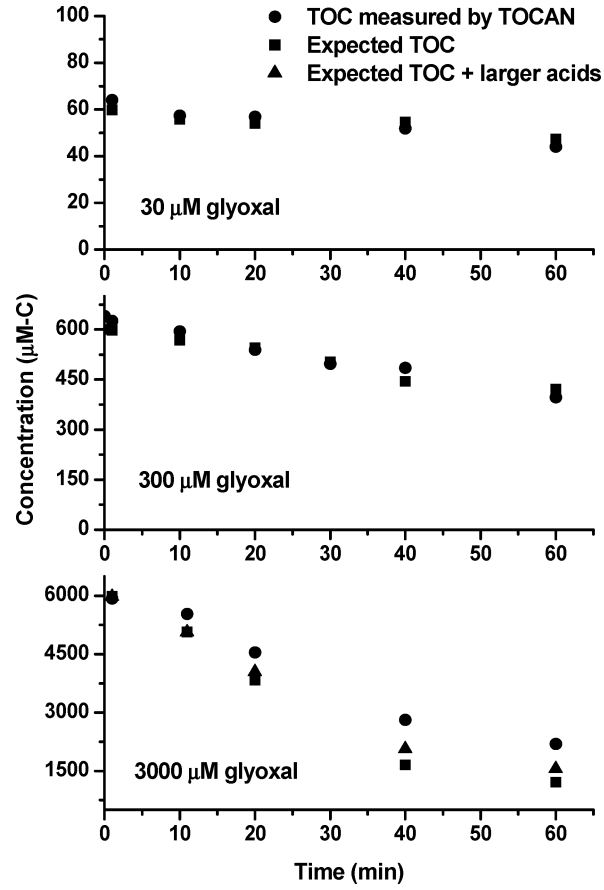

FIGURE 3. Measured total organic carbon (TOC) and reconstructed TOC. Circles (●) are total TOC measured by the TOC-5000A analyzer. Reconstructed TOC is calculated by compound concentration times number of carbon in compound. Squares (■) are the quantified organic carbon (sum of carbon in oxalic, malonic, and succinic acids measured by IC and modeled glyoxal and glyoxylic acid). Triangles (▲) (expected TOC) indicate quantified organic carbon minus malonic and succinic acids in 3000 μM experiments.

oxalic acid concentrations were higher than reported previously (*18*). We believe that is because large differences in the void volume between samples and standards in the previous analysis (conducted by HPLC-UV−vis, not IC) altered the baseline near the oxalic acid peak.

The dilute aqueous chemistry model (Table 1) successfully reproduced oxalic acid time profiles in 30 μM experiments conducted without H_2SO_4 (Figure 2). Total organic carbon (TOC) analysis (Figure 3) shows that the model is capable of predicting the organic carbon content of the reaction vessel in 30 and 300 μM experiments. This suggests that oxalic acid production from glyoxal can be predicted at cloud-relevant concentrations without considering the formation of higher molecular weight products.

At higher concentrations (3000 μM), measured oxalic acid concentrations were lower and peaked later than the model predicted, and expected organic carbon accounted for less than 60% of the measured TOC in 40 and 60 min samples. A similar observation has been made for glycoaldehyde and OH radical (*23*). The ESI-MS negative mode spectrum of the 3000 μM glyoxal + OH radical products (20 min) is more complex and contains more higher molecular weight compounds than the spectrum obtained 20 min into the 30 μM experiment (Figure 4). In the mass range from 50 to 500 amu, m/z^- 188, 271, and 279 were the median ions present in the 30, 300, and 3000 μM experiments, respectively. A total of 76, 161, and 204 ions were detected, respectively, in

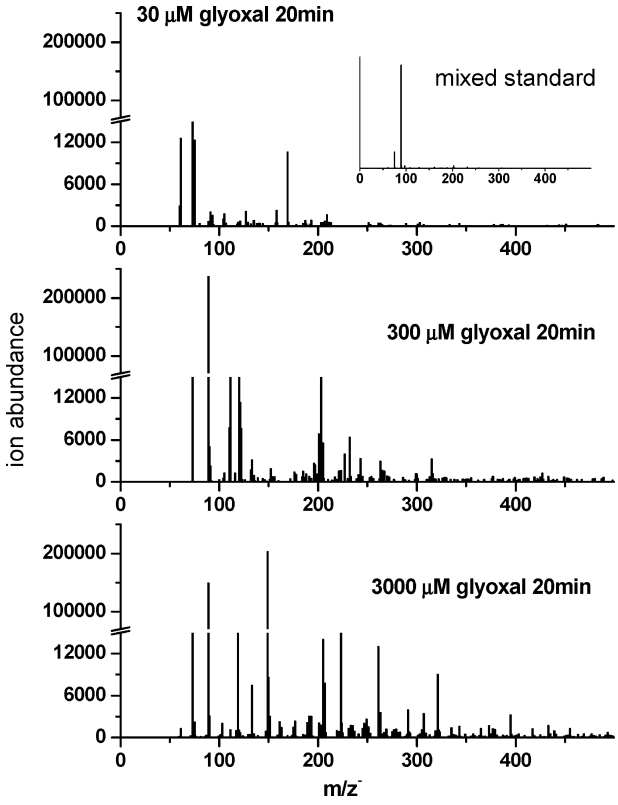

FIGURE 4. ESI-MS negative ionization mode spectra of samples taken from glyoxal + OH radical batch reactions (20 min reaction time). From top to bottom: 30 μM glyoxal + OH radical (0.15 mM H_2O_2 + UV), 300 μM glyoxal + OH radical (1.5 mM H_2O_2 + UV), and 3000 μM glyoxal + OH radical (15 mM H_2O_2 + UV). A mass spectrum of mixed standard is shown in the inset (hydrogen peroxide, glyoxal, formic acid, glycolic acid, glyoxylic acid, and oxalic acid each 200 μM, a similar concentration as observed for oxalic acid at 20 min, 3000 μM experiment).

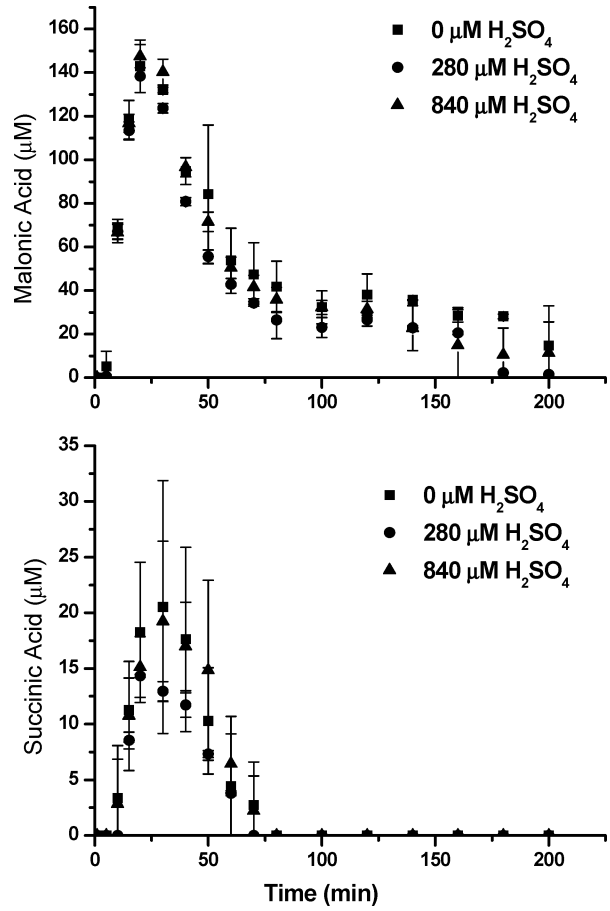

FIGURE 5. Malonic plus tartaric acid and succinic plus malic acid in 3000 μM glyoxal + OH radical experiments with and without H_2SO_4. Note malonic acid coelutes with tartaric acid and succinic acid coelutes with malic acid. Peaks were quantified on the basis of malonic acid and succinic acid standards.

the 30, 300, and 3000 μM experiments. The negative mode spectrum of a mixed standard that included all expected products and precursors was quite simple, suggesting that the complexity seen in samples was not an artifact of the electrospray ionization process (Figure 4 insert; glyoxal, H_2O_2, glyoxylic acid, oxalic acid, formic acid, and glycolic acid, each at 200 μM; these products are 20−300 μM in 3000 μM glyoxal experiments at 20 min). This complexity was not seen in control experiments, indicating that the higher molecular weight products are only formed in the presence of the OH radical. The larger number and complexity of higher molecular weight products with increasing precursor concentration could explain the gap between measured TOC and carbon in predicted products and is consistent with the possibility that formation of higher molecular weight products or oligomers plays an increasingly important role as concentrations increase. The formation of higher molecular weight products could explain the lower measured oxalic acid concentrations and slower production rate relative to predictions in the 3000 μM experiments. The trends exhibited in Figures 2−4 suggest that it will be necessary to account for the formation of higher molecular weight products in order to accurately predict oxalic acid formation (and aqueous-phase SOA formation) from glyoxal + OH radical in aerosol water, where glyoxal concentrations can be 3 orders of magnitude greater than those in our highest experiments.

Additional Carboxylic Acids and Oligomer Formation. IC chromatograms of 30 and 300 μM experiments are relatively simple, only showing organic acids predicted by the explicit dilute aqueous chemistry model. In contrast, several additional peaks not found in control experiments showed clear growth and decay in IC analysis of 3000 μM experiments (Figure S3 of the Supporting Information). Specifically, small peaks with the same retention time as malonic plus tartaric acid and succinic plus malic acid standards were observed. A peak with the retention time expected for mesoxalic acid was also found. Several small peaks that eluted after 30 min are consistent with the presence of tricarboxylic acids on the basis of on the separation mechanism of the column. Additionally, the presence of compounds with the exact elemental formulas as succinic acid (m/z^- 117.0193, $C_4H_5O_4^-$), malonic acid (m/z^- 103.0036, $C_3H_3O_4^-$), malic acid (m/z^- 133.01422, $C_4H_5O_5^-$), tartaric acid (149.00907, $C_4H_5O_6^-$), and mesoxalic acid (m/z^- 116.98294, $C_3H_1O_5^-$) in the FT-ICR mass spectra provides strong support for the formation of these compounds in 3000 μM experiments. These ions were not found in analyses of mixed standards or in control experiments. Figure 5 shows time profiles for malonic plus tartaric acids (quantified as malonic acid) and succinic plus malic acid (quantified as succinic acid). The relatively high concentrations of these compounds in 3000 μM experiments suggest that compounds with more than two carbon atoms could be important products in glyoxal oxidation at the considerably higher concentrations observed in aerosol water. The carbon balance for 3000 μM experiments is improved by including malonic acid and succinic acid, but the carbon in the sum of quantified species

TABLE 2. Oligomer Series Found by FT-ICR-MS Negative Ionization Mode in a Sample Taken at 30 min Reaction Time (Experiment 13)[a]

parent acid	glyoxylic acid		oxalic acid		malonic acid	
subunit	chemical formula	m/z^-	chemical formula	m/z^-	chemical formula	m/z^-
	$C_2H_1O_3$	72.99297	$C_2H_1O_4$	88.98803	$C_3H_3O_4$	103.0037
s_1	$C_5H_5O_5$	145.0142	$C_5H_5O_6$	161.0091	$C_6H_7O_6$	175.0248
s_2	$C_6H_5O_7$	189.0041	$C_6H_5O_8$	204.9990	$C_7H_7O_8$	219.0146
s_3	$C_6H_5O_8$	204.9990	$C_6H_5O_9$	220.9939	$C_7H_7O_9$	235.0095
$2s_1$	$C_8H_9O_7$	217.0354	$C_8H_9O_8$	233.0303	$C_9H_{11}O_8$	247.046
$s_1+ s_2$	$C_9H_9O_9$	261.0252	$C_9H_9O_{10}$	277.0201	$C_{10}H_{11}O_{10}$	291.0357
$s_1+ s_3$	$C_9H_9O_{10}$	277.0201	$C_9H_9O_{11}$	293.0149	$C_{10}H_{11}O_{11}$	307.0305
$3s_1$	$C_{11}H_{13}O_9$	289.0564	$C_{11}H_{13}O_{10}$	305.0512		
$2s_2$	$C_{10}H_9O_{11}$	305.0149	$C_{10}H_9O_{12}$	321.0097	$C_{11}H_{11}O_{12}$	335.0254
$s_2+ s_3$	$C_{10}H_9O_{12}$	321.0097	$C_{10}H_9O_{13}$	337.0049	$C_{11}H_{11}O_{13}$	351.0204
$2s_1+ s_2$	$C_{12}H_{13}O_{11}$	333.0464	$C_{12}H_{13}O_{12}$	349.0412	$C_{13}H_{15}O_{12}$	363.0568
$2s_3$	$C_{10}H_9O_{13}$	337.0049	$C_{10}H_9O_{14}$	352.9997	$C_{11}H_{11}O_{14}$	367.0153
$2s_1+ s_3$	$C_{12}H_{13}O_{12}$	349.0412	$C_{12}H_{13}O_{13}$	365.0360	$C_{13}H_{15}O_{13}$	379.0517
$4s_1$	$C_{14}H_{17}O_{11}$	361.0775	$C_{14}H_{17}O_{12}$	377.0724		
$s_1+ 2s_2$	$C_{13}H_{13}O_{13}$	377.0361	$C_{13}H_{13}O_{14}$	393.0310	$C_{14}H_{15}O_{14}$	407.0466
$s_1+ s_2+ s_3$	$C_{13}H_{13}O_{14}$	393.0310	$C_{13}H_{13}O_{15}$	409.026	$C_{14}H_{14}O_{15}$	423.0418
$3s_1+ s_2$	$C_{15}H_{17}O_{13}$	405.0674	$C_{15}H_{17}O_{14}$	421.0624		
$2s_3+ s_1$	$C_{13}H_{13}O_{15}$	409.026				
$3s_2$	$C_{14}H_{13}O_{15}$	421.0267				
$3s_1+ s_3$	$C_{15}H_{17}O_{14}$	421.0624	$C_{15}H_{17}O_{15}$	437.0573		
$2s_1+ 2s_2$	$C_{16}H_{17}O_{15}$	449.0575				

[a] Products formed from parent acids are categorized by addition of subunits: s_1 denotes $C_3H_4O_2$, s_2 denotes $C_4H_4O_4$, and s_3 denotes $C_4H_4O_5$. All compounds are shown as an anion with one negative charge via losing a proton during the ionization process. (Around 45% of the ion abundance in this sample is accounted for by products in this table.).

TABLE 3. Oligomer Series Found by FT-ICR-MS Negative Ionization Mode in a Sample Taken at 30 min Reaction Time (Experiment 13)[a]

parent acid	succinic acid		malic acid		tartaric acid	
subunit	chemical formula	m/z^-	chemical formula	m/z^-	chemical formula	m/z^-
	$C_4H_5O_4$	117.01929	$C_4H_5O_5$	133.01422	$C_4H_5O_6$	149.00907
s_1	$C_7H_9O_6$	189.04051	$C_7H_9O_7$	205.0354	$C_7H_9O_8$	221.03029
s_2	$C_8H_9O_8$	233.0303	$C_8H_9O_9$	249.0252	$C_8H_9O_{10}$	265.02011
s_3	$C_8H_9O_9$	249.0252	$C_8H_9O_{10}$	265.02011	$C_8H_9O_{11}$	281.01495
$2s_1$			$C_{10}H_{13}O_9$	277.05649	$C_{10}H_{13}O_{10}$	293.05128
$s_1+ s_2$	$C_{11}H_{13}O_{10}$	305.05123	$C_{11}H_{13}O_{11}$	321.04609	$C_{11}H_{13}O_{12}$	337.04124
$s_1+ s_3$	$C_{11}H_{13}O_{11}$	321.04609	$C_{11}H_{13}O_{12}$	337.04124	$C_{11}H_{13}O_{13}$	353.03607
$3s_1$			$C_{13}H_{17}O_{11}$	349.07748	$C_{13}H_{17}O_{12}$	365.07235
$2s_2$	$C_{12}H_{13}O_{12}$	349.0412	$C_{12}H_{13}O_{13}$	365.03604	$C_{12}H_{13}O_{14}$	381.03092
$s_2+ s_3$	$C_{12}H_{13}O_{13}$	365.03604	$C_{12}H_{13}O_{14}$	381.03092	$C_{12}H_{13}O_{15}$	397.02577
$2s_1+ s_2$	$C_{14}H_{17}O_{12}$	377.07244	$C_{14}H_{17}O_{13}$	393.06719	$C_{14}H_{17}O_{14}$	409.06211
$2s_3$	$C_{12}H_{13}O_{14}$	381.03092	$C_{12}H_{13}O_{15}$	397.02577		
$2s_1+ s_3$	$C_{14}H_{17}O_{13}$	393.06719	$C_{14}H_{17}O_{14}$	409.06211	$C_{14}H_{17}O_{15}$	425.05733
$4s_1$						
$s_1+ 2s_2$	$C_{15}H_{17}O_{14}$	421.06241	$C_{15}H_{17}O_{15}$	437.05727		
$s_1+ s_2+ s_3$	$C_{15}H_{17}O_{15}$	437.05727				

[a] Products formed from parent acids are categorized by addition of subunits: s_1 denotes $C_3H_4O_2$, s_2 denotes $C_4H_4O_4$, and s_3 denotes $C_4H_4O_5$. All compounds are shown as an anion with one negative charge via losing a proton during the ionization process. (Around 45% of the ion abundance in this sample is accounted for by products in this table.).

is still ~25% less than measured TOC in 40 and 60 min samples (Figure 3).

Succinic acid is a key intermediate in the oligomer formation mechanism proposed for aqueous OH radical oxidation of methylglyoxal and glycoaldehyde (*23, 27*). As previously reported for methylglyoxal (*24*), pyruvic acid (*22*), and glycolaldehyde (*23*), the mass spectra of 3000 μM glyoxal + OH radical samples exhibit a "haystack" pattern with mass differences of 12, 14, and 16 amu, respectively (Figure 4). Similar to methylglyoxal and glycolaldehyde, repeated addition of a subunit (s_1) with the elemental formula $C_3H_4O_2$ and molecular weight 72.0211 to organic acids was found (Table 2). These products did not form in the absence of OH radicals. The formation of oligoesters by repeated addition of s_1 was verified by MS-MS in methylglyoxal experiments (*27*). Oligoesters might form through esterification (condensation) reactions or radical−radical reactions, suggesting that s_1 could be a radical or a compound with alcohol and acid functionalities. Unlike glyoxal oligomers formed through hemiacetal formation, we expect that oligomers from OH radical reactions will be irreversibly formed. In addition, in this work, the repeated addition of subunits with molecular formulas $C_4H_4O_4$ (s_2) and $C_4H_4O_5$ (s_3) (molecular weights 116.0110 and 132.0058, respectively) to parent compounds could also be seen in the FT-ICR-MS analysis of 3000 μM glyoxal + OH radical samples (Tables 2,3). For example, oxalic acid ($C_2H_2O_4$) was found to add 1−4 different or same subunits, forming $C_2H_2O_4-C_3H_4O_2$, $C_2H_2O_4-(C_3H_4O_2)_2$,

$C_2H_2O_4-(C_3H_4O_2)_3$, etc. It should be noted that oligomeric products from these two subunits account for only a portion of the FT-ICR-MS signal. About 45% of the ion abundance in the 30 min sample is accounted for by the products listed in Tables 2 and 3. The higher molecular weight carboxylic acids and oligomers identified by IC and/or FT-ICR-MS could partially account for the missing carbon in the 3000 μM experiment. This work suggests that product complexity and oligomer formation becomes increasingly important as precursor concentrations increase from those typically seen in clouds to those typically seen in aerosol water.

This work provides insights pertaining to the aqueous OH radical oxidation of glyoxal at cloud- and aerosol-relevant concentrations. At cloud-relevant concentrations the Lim et al. (*25*) dilute aqueous chemistry model successfully predicts oxalic acid formation and total carbon. As precursor concentrations increase, SOA prediction is complicated by the increasing formation of higher molecular weight products; peak oxalic acid concentrations occur later in the reaction sequence, and higher molecular weight products, including >C2 organic acids and oligomers form. These products are also expected to contribute to SOA. In wet aerosols, where glyoxal also reacts with species other than the OH radical, glyoxal chemistry could be even more complex (*28*−*31*). Thus, more research is needed to build a chemical model capable of accurately predicting SOA formation from glyoxal in wet aerosols. This work suggests acidic sulfate has only a small effect on oxalic acid production at cloud- and fog-relevant conditions; its effect on aqueous oligomers and organosulfur species formation was not explored nor was its effect at aerosol-relevant concentrations. In some smog chamber experiments, reactive uptake of glyoxal seems to be enhanced by acidic sulfate (*32, 33*). This does not necessarily conflict with our findings because the sulfate and H^+ concentrations in wet aerosols are orders of magnitudes higher than in our experiments.

Acknowledgments

This research was supported by the National Science Foundation (NSF) (000433435), National Oceanic and Atmospheric Administration (NOAA) (NA07OAR4310279), and U.S. Environmental Protection Agency (EPA) Science to Achieve Results (STAR) program (R833751). The authors acknowledge Dr. Melissa Soule, Dr. Elizabeth Kujawinski, and the funding sources of the WHOI FT-MS Users' Facility (NSF OCE-0619608 and the Gordon and Betty Moore Foundation). Any opinions, findings, and conclusions or recommendations expressed in this material are those of the authors and do not necessarily reflect the views of the NSF, NOAA, or EPA; no official endorsement should be inferred. The authors thank Ron Lauck, Ann Marie Carlton, and Yong Bin Lim for laboratory assistance and invaluable discussions.

Supporting Information Available

Analytical details, QA/QC, measurement of H_2O_2 photolysis (Figure S1), decay of glyoxal (Figure S2), and IC chromatogram of a sample (Figure S3). This material is available free of charge via the Internet at http://pubs.acs.org.

Literature Cited

(1) Kanakidou, M.; Seinfeld, J. H.; Pandis, S. N.; Barnes, I.; Dentener, F. J.; Facchini, M. C.; Van Dingenen, R.; Ervens, B.; Nenes, A.; Nielsen, C. J.; Swietlicki, E.; Putaud, J. P.; Balkanski, Y.; Fuzzi, S.; Horth, J.; Moortgat, G. K.; Winterhalter, R.; Myhre, C. E. L.; Tsigaridis, K.; Vignati, E.; Stephanou, E. G.; Wilson, J. Organic aerosol and global climate modelling: A review. *Atmos. Chem. Phys.* **2005**, *5*, 1053–1123.

(2) Poschl, U. Atmospheric aerosols: Composition, transformation, climate, and health effects. *Angew. Chem., Int. Ed.* **2005**, *44* (46), 7520–7540.

(3) Volkamer, R.; Jimenez, J. L.; San Martini, F.; Dzepina, K.; Zhang, Q.; Salcedo, D.; Molina, L. T.; Worsnop, D. R.; Molina, M. J., Secondary organic aerosol formation from anthropogenic air pollution: Rapid and higher than expected. *Geophys. Res. Lett.* **2006**, *33*, L17811, DOI:10.1029/2006GL026899.

(4) Heald, C. L.; Jacob, D. J.; Park, R. J.; Russell, L. M.; Huebert, B. J.; Seinfeld, J. H.; Liao, H.; Weber, R. J., A large organic aerosol source in the free troposphere missing from current models. *Geophys. Res. Lett.* **2005**, *32*, L18809, DOI:10.1029/2005GL023831.

(5) Chebbi, A.; Carlier, P. Carboxylic acids in the troposphere, occurrence, sources, and sinks: A review. *Atmos. Environ.* **1996**, *30* (24), 4233–4249.

(6) Heald, C. L.; Jacob, D. J.; Turquety, S.; Hudman, R. C.; Weber, R. J.; Sullivan, A. P.; Peltier, R. E.; Atlas, E. L.; de Gouw, J. A.; Warneke, C.; Holloway, J. S.; Neuman, J. A.; Flocke, F. M.; Seinfeld, J. H., Concentrations and sources of organic carbon aerosols in the free troposphere over North America. *J. Geophys. Res.* **2006**, *111*, D23s47, DOI:10.1029/2006JD007705.

(7) Sorooshian, A.; Lu, M.-L.; Brechtel, F. J.; Jonsson, H.; Feingold, G.; Flagan, R. C.; Seinfeld, J. H. On the source of organic acid aerosol layers above clouds. *Environ. Sci. Technol.* **2007**, *41* (13), 4647–4654.

(8) Sorooshian, A.; Ng, N. L.; Chan, A. W. H.; Feingold, G.; Flagan, R. C.; Seinfeld, J. H., Particulate organic acids and overall water-soluble aerosol composition measurements from the 2006 Gulf of Mexico Atmospheric Composition and Climate Study (GoMACCS). *J. Geophys. Res.* **2007**, *112*, D13201, DOI:10.1029/2007JD008537.

(9) Blando, J. D.; Turpin, B. J. Secondary organic aerosol formation in cloud and fog droplets: A literature evaluation of plausibility. *Atmos. Environ.* **2000**, *34*, 1623–1632.

(10) Gelencser, A.; Varga, Z. Evaluation of the atmospheric significance of multiphase reactions in atmospheric secondary organic aerosol formation. *Atmos. Chem. Phys.* **2005**, *5*, 2823–2831.

(11) Limbeck, A.; Puxbaum, H.; Otter, L.; Scholes, M. C. Semivolatile behavior of dicarboxylic acids and other polar organic species at a rural background site (Nylsvley, RSA). *Atmos. Environ.* **2001**, *35*, 1853–1862.

(12) Fu, T.-M.; Jacob, D. J.; Wittrock, F.; Burrows, J. P.; Vrekoussis, M.; Henze, D. K., Global budgets of atmospheric glyoxal and methylglyoxal, and implications for formation of secondary organic aerosols. *J. Geophys. Res.* **2008**, *113*, D15303, DOI:10.1029/2007JD009505.

(13) Feierabend, K. J.; Zhu, L.; Talukdar, R. K.; Burkholder, J. B. Rate coefficients for the OH + HC(O)C(O)H (glyoxal) reaction between 210 and 390 K. *J. Phys. Chem. A* **2008**, *112* (1), 73–82.

(14) Volkamer, R.; San Martini, F.; Molina, L. T.; Salcedo, D.; Jimenez, J. L.; Molina, M. J. A missing sink for gas-phase glyoxal in Mexico City: Formation of secondary organic aerosol. *Geophys. Res. Lett.* **2007**, *34*, L19807, DOI:10.1029/2007GL030752.

(15) Schweitzer, F.; Magi, L.; Mirabel, P.; George, C. Uptake rate measurements of methanesulfonic acid and glyoxal by aqueous droplets. *J. Phys. Chem. A* **1998**, *102* (3), 593–600.

(16) Ip, H. S. S.; Huang, X. H. H.; Yu, J. Z. Effective Henry's law constants of glyoxal, glyoxylic acid, and glycolic acid. *Geophys. Res. Lett.* **2009**, *36*, L01802, DOI:10.1029/2008GL036212.

(17) Munger, J. W.; Jacob, D. J.; Daube, B. C.; Horowitz, L. W. Formaldehyde, glyoxal, and methylglyoxal in air and cloudwater at a rural mountain site in central Virginia. *J. Geophys. Res.* **1995**, *100* (D5), 9325–9333.

(18) Carlton, A. G.; Turpin, B. J.; Altieri, K. E.; Seitzinger, S.; Reff, A.; Lim, H.-J.; Ervens, B. Atmospheric oxalic acid and SOA production from glyoxal: Results of aqueous photooxidation experiments. *Atmos. Environ.* **2007**, *41* (35), 7588–7602.

(19) Carlton, A. G.; Turpin, B. J.; Altieri, K. E.; Seitzinger, S. P.; Mathur, R.; Roselle, S. J.; Weber, R. J. CMAQ model performance enhanced when in-cloud secondary organic aerosol is included: Comparisons of organic carbon predictions with measurements. *Environ. Sci. Technol.* **2008**, *42* (23), 8798–8802.

(20) Jang, M.; Czoschke, N. M.; Lee, S.; Kamens, R. M. Heterogeneous atmospheric aerosol production by acid-catalyzed particle-phase reactions. *Science* **2002**, *298*, 814–817.

(21) Iinuma, Y.; Müller, C.; Böge, O.; Gnauk, T.; Herrmann, H. The formation of organic sulfate esters in the limonene ozonolysis secondary organic aerosol (SOA) under acidic conditions. *Atmos. Environ.* **2007**, *41* (27), 5571–5583.

(22) Carlton, A. G.; Turpin, B. J.; Lim, H.-J.; Altieri, K. E.; Seitzinger, S., Link between isoprene and secondary organic aerosol (SOA): Pyruvic acid oxidation yields low volatility organic acids in clouds. *Geophys. Res. Lett.* **2006**, *33*.
(23) Perri, M. J.; Seitzinger, S.; Turpin, B. J. Secondary organic aerosol production from aqueous photooxidation of glycolaldehyde: Laboratory experiments. *Atmos. Environ.* **2009**, *43* (8), 1487–1497.
(24) Altieri, K. E.; Carlton, A. G.; Lim, H.-J.; Turpin, B. J.; Seitzinger, S. P. Evidence for oligomer formation in clouds: Reactions of isoprene oxidation products. *Environ. Sci. Technol.* **2006**, *40* (16), 4956–4960.
(25) Lim, H. J.; Carlton, A. G.; Turpin, B. J. Isoprene forms secondary organic aerosol through cloud processing: Model simulations. *Environ. Sci. Technol.* **2005**, *39*, 4441–4446.
(26) Ervens, B.; Feingold, G.; Frost, G. J.; Kreidenweis, S. M. A modeling study of aqueous production of dicarboxylic acids: 1. Chemical pathways and speciated organic mass production. *J. Geophys. Res.* **2004**, *109*, D15205, DOI:10.1029/2003JD004387.
(27) Altieri, K. E.; Seitzinger, S. P.; Carlton, A. G.; Turpin, B. J.; Klein, G. C.; Marshall, A. G. Oligomers formed through in-cloud methylglyoxal reactions: Chemical composition, properties, and mechanisms investigated by ultra-high resolution FT-ICR mass spectrometry. *Atmos. Environ.* **2008**, *42* (7), 1476–1490.
(28) Noziere, B.; Dziedzic, P.; Cordova, A. Products and kinetics of the liquid-phase reaction of glyoxal catalyzed by ammonium ions (NH_4^+). *J. Phys. Chem. A* **2008**, *113* (1), 231–237.
(29) Shapiro, E. L.; Szprengiel, J.; Sareen, N.; Jen, C. N.; Giordano, M. R.; McNeill, V. F. Light-absorbing secondary organic material formed by glyoxal in aqueous aerosol mimics. *Atmos. Chem. Phys.* **2009**, *9* (7), 2289–2300.
(30) De Haan, D. O.; Tolbert, M. A.; Jimenez, J. L., Atmospheric condensed-phase reactions of glyoxal with methylamine. *Geophys. Res. Lett.* **2009**, *36*.
(31) Galloway, M. M.; Chhabra, P. S.; Chan, A. W. H.; Surratt, J. D.; Flagan, R. C.; Seinfeld, J. H.; Keutsch, F. N. Glyoxal uptake on ammonium sulphate seed aerosol: Reaction products and reversibility of uptake under dark and irradiated conditions. *Atmos. Chem. Phys.* **2009**, *9* (10), 3331–3345.
(32) Corrigan, A. L.; Hanley, S. W.; De Haan, D. O. Uptake of glyoxal by organic and inorganic aerosol. *Environ. Sci. Technol.* **2008**, *42* (12), 4428–4433.
(33) Liggio, J.; Li, S.-M.; McLaren, R. Heterogeneous reactions of glyoxal on particulate matter: Identification of acetals and sulfate esters. *Environ. Sci. Technol.* **2005**, *39* (6), 1532–1541.
(34) Leitzke, A.; Reisz, E.; Flyunt, R.; von Sonntag, C. The reactions of ozone with cinnamic acids: Formation and decay of 2-hydroxyperoxy-2-hydroxyacetic acid. *J. Chem. Soc., Perkin Trans. 2* **2001**, (5), 793–797.

ES901742F